Chem

CellPress

Article

Guest binding is governed by multiple stimuli in low-symmetry metal-organic cages containing bis-pyridyl(imine) vertices

Yuchong Yang,[1] Tanya K. Ronson,[1] Paula C.P. Teeuwen,[1] Yuyin Du,[1] Jieyu Zheng,[1] David J. Wales[1,*] & Jonathan R. Nitschke[1,2,*]

[1]Yusuf Hamied Department of Chemistry, University of Cambridge, Lensfield Road, Cambridge, CB2 1EW, UK.

[2]Lead contact

*Correspondence: jrn34@cam.ac.uk, dw34@cam.ac.uk

SUMMARY

Inspired by natural systems, metal-organic cages with well-defined shapes and cavities can be tuned for different guest-binding functions. Here we report the construction of two types of cage framework: an $M^{II}_{12}L_8$ (M = Zn^{II}, Co^{II}) *pseudo*-cuboctahedral architecture 1, and a rarer $M^{II}_{9}L_8$ (M = Zn^{II}, Co^{II}) *pseudo*-Johnson-solid-type (J_{51}) framework 2. Both structures form from the same boron-containing triamine subcomponent, and each one incorporates hexacoordinate metal vertices chelated by only two bidentate pyridyl(imine) arms. Such metal vertices provide the cages with the flexibility required to form lower symmetry architectures, and also facilitate reversible disassembly in response to fluoride. These cages were also shown to respond to other chemical stimuli enabling transformation between cage structures. Cage 1 bound different guest molecules, including the anticancer drug paclitaxel, *C*-methylcalix[4]resorcinarene, and tetraphenylborates. The release of paclitaxel by 1 was stimulated by fluoride or chloride, highlighting the potential for applications in natural product separation and drug delivery.

Keywords: self-assembly, metal-organic cages, host-guest chemistry, structural transformations, fluoride response.

INTRODUCTION

Biomolecular capsules, such as viral capsids and ferritin protein cages, consist of identical subunits that tile the surface of a polyhedron.[1–3] Inspired by these natural systems, a variety of artificial metal-organic cages with well-defined polyhedral shapes and cavities have been developed, including Platonic solids, Archimedean solids,[4–13] and prisms.[14,15] Such high-symmetry metal-organic polyhedra may be constructed using relatively simple design strategies, as their building blocks occupy only one or two symmetry-equivalent environments. Self-assembled biological encapsulants exceed the complexity of synthetic examples, particularly in their ability to adopt lower-symmetry architectures.[16] The Johnson solids,[17,18] a series of 92 convex regular-faced non-uniform polyhedra, represent attractive synthetic hosts for binding low-symmetry guests.

Metal-organic cages have demonstrated utility in fields that include capturing reactive species,[19,20] chemical purifications,[21-23] enantioselective sensing and separations,[24,25] and catalysis.[26,27] Cages have been demonstrated to respond to various stimuli, such as changes in pH,[28,29] light,[30-32] concentration,[33] guest binding,[34-36] subcomponent/ligand exchange,[37-39] redox reactions[40,41] and post-assembly modifications,[42–45] which can further tune their structures and properties for targeted applications. These stimuli can trigger breaking and reforming of the different bonds that hold the cages together, resulting in structural changes

and potentially bringing about guest release and uptake. Thus, developing new types of stimuli can expand the range of cage applications.

Here we report the preparation of $M^{II}_{12}L_8$ *pseudo*-cuboctahedral cage framework **1** (Figure 1), where each metal ion vertex is chelated by only two pyridyl(imine) units and two monodentate ancillary ligands. From the same set of subcomponents used to prepare **1**, a suitably-sized anionic template[46,47] instead produced *pseudo*-Johnson-type (J_{51}) cage **2** with an $M^{II}_9L_8$ framework,[48,49] which incorporates both bis-pyridyl(imine) and tris-pyridyl(imine) chelated metal vertices. Owing to unsaturated bis-pyridyl(imine) vertices, both **1** and **2** disassembled reversibly upon fluoride addition, and were regenerated upon the addition of Ca^{2+}. Cage **1** bound guest molecules that include paclitaxel, highlighting the potential of this fluoride-responsive system for natural product separation and drug delivery.

RESULTS AND DISCUSSION

Construction of *pseudo*-cuboctahedral cage 1 and *pseudo*-Johnson-type (J_{51}) cage 2

As shown in Figure 1, subcomponent **A** (8 equiv) reacted with subcomponent **B** (2-formyl-5-methoxypyridine, 24 equiv) and zinc(II) trifluoromethanesulfonate or cobalt(II) perchlorate (12 equiv) in acetonitrile to produce either **Zn-1** or **Co-1** (Figures S1-S7 and S9). The $M^{II}_{12}L_8$ compositions of these structures were confirmed by electrospray ionization mass spectrometry (ESI-MS) (Figure 1D and Figures S10 and S11). All of the ^{1}H NMR signals assigned to **Zn-1** exhibited the same diffusion-ordered spectroscopy (DOSY) diffusion coefficient, indicating a hydrodynamic diameter of 39.1 Å (Figures 1B and Figure S8). This diameter is consistent with the size of **1** observed in the solid-state structure of *pseudo*-cuboctahedral cage **Zn-1**, as determined by single-crystal X-ray diffraction (XRD) at Diamond Light Source,[50] shown in Figure 1C.

The twelve Zn^{II} centers of **Zn-1** form a distorted cuboctahedral framework (Figure 1A), with *tris*-bidentate ligands panelling the eight triangular cuboctahedron faces, leaving the six square faces vacant. Steric hindrance between the pyridyl ring of one ligand and the methyl group of an adjacent ligand (Figures 1C and Figure S77) results in a configuration where half of the ligands adopt a clockwise orientation, with the other half anticlockwise, consistent with the observation of two sets of peaks in the ^{1}H NMR spectrum (Figure 1B and C). The metal centers within **1** possess the same handedness, with non-crystallographic T_d symmetry, which is lower in symmetry than the reported cuboctahedral cages with O_h symmetry,[51] as confirmed by NMR spectroscopy (Figures S1-S7).

The electron-withdrawing effects of the methoxy group *meta* to the pyridine nitrogen atom on each ligand of **1** are expected to weaken the ligand strength. This weakened ligand strength may contribute to only two pyridyl(imine) ligand arms chelating to each 6-coordinate metal-ion vertex, with the other two coordination sites being occupied acetonitrile molecules or counter anions, as observed in the crystal.[52,53] The angle between the chelate planes of the two pyridyl(imine) ligands at each vertex is thus approximately 96°, giving rise to the *pseudo*-cuboctahedral geometry of cage framework **1**.

As shown in Figure 2, subcomponent **A** (8 equiv) reacted with subcomponent **B** (24 equiv) and Zn(II) and Co(II) bis(trifluoromethanesulfonimide) (triflimide or Tf_2N^-, 9 equiv) in acetonitrile to produce $M^{II}_9L_8$ **Zn-2** or **Co-2**. In contrast to the construction of cage **1**, the main difference in this case was the use of Tf_2N^- counter anions rather than TfO^- or ClO_4^-. The geometries of these two cage assemblies were inferred based upon NMR spectroscopy and ESI-MS (Figures S12-S25). The ^{1}H NMR spectra of **Zn-2** and **Co-2** were complex, indicating low symmetry (Figures S12 and S22). Twelve imine peaks were observed in the ^{1}H-^{13}C HSQC spectra of **Zn-2** (24 imine bonds in total), consistent with C_2 symmetry. Similarly, twelve imine peaks were also observed in the paramagnetic ^{1}H NMR spectra of **Co-2**.[54] According to the NMR spectra and ESI-MS results, we hypothesize the structure shown in Figures 2B and S69 for **Co-2**. Six Δ-tris-pyridyl(imine) metal vertices are separated by a C_2 axis, which are connected by 2 Λ-bis-pyridyl(imine) metal vertices and one Δ-bis-pyridyl(imine) metal vertex. All ^{1}H NMR signals assigned to **Zn-2** displayed the same DOSY diffusion coefficient, corresponding to a solvodynamic diameter of 38.1 Å (Figures 2C and S19), consistent with the GFN2-xTB structure shown in Figures 2B and S19. The ^{19}F NMR spectra of **Zn-2** and **Co-2** exhibit signals assigned

to both free and encapsulated Tf_2N^-, as shown in Figures S14 and S23. **Zn-2** and **Co-2** formed only in the presence of Tf_2N^-, indicating that Tf_2N^- may template the formation of the framework of **2**.

Many attempts at growing crystals of cage **2** suitable for X-ray diffraction were unsuccessful, hence we have employed calculations to identify the lowest-energy configuration of framework **2**. Energy minimisations of the different possible configurations of the $M^{II}_9L_8$ *pseudo*-Johnson-type (J_{51}) coordination cage framework **2** were carried out at the GFN2-xTB level using the OPTIM interface[55] to the *xtb* program. These results are shown in Figure 2B. Four pairs of enantiomers of **Zn-2** were examined, as shown in Figures S78-S81. In comparing the minimised energies of these possible structures, one was found to be reasonable and lower in energy than the others by 11, 35 and 56 kJ mol^{-1}, respectively, suggesting that **Zn-2** may adopt the structure shown in Figure 2C. In this cage structure, all boron centers adopt a planar sp^2 configuration, and all the metal centers except for two have the same handedness, producing C_2 symmetry. The farthest distance between two protons in the optimised structure is 39.1 Å, consistent with the DOSY hydrodynamic radius of 38.1 Å obtained for **Zn-2**.

Fluoride-induced reversible cage disassembly

The fluoride-triggered disassembly of **Zn-1** and **Co-1** was investigated by ^{1}H NMR (Figures S34 and S39). After the addition of 24 equiv of tetrabutylammonium fluoride (TBAF) to **Zn-1** and **Co-1** in CD_3CN, the yellow cage solution lightened in colour and developed a precipitate within two minutes. The ^{1}H NMR signals became broad, and signals corresponding to free 5-methoxypicolinaldehyde were observed for both **Zn-1** and **Co-1**, suggesting cage disassembly. This fluoride-induced cage disassembly was not observed for cages with tris(bidentate)-chelated vertices.[43] No ^{19}F NMR signals were observed between −160 and −170 ppm, consistent with the absence of B←F^- adducts. Following the addition of a further 8 equiv of TBAF, for a total of 32 equiv, a broad ^{19}F signal was observed at −168.7 ppm, indicating the formation of a B←F^- adduct of the free ligands. We thus infer that F^- first coordinates to the bis(bidentate)-chelated Zn^{II} and Co^{II} cage vertices to form poorly-soluble ZnF_2 and CoF_2, thus resulting in cage disassembly.

The reversibility of the fluoride-responsive disassembly of cages was explored through the addition of Ca^{2+}, which can trap fluoride by precipitation of highly insoluble CaF_2. After heating for 5 min at 50 ˚C, the addition of excess $Ca(OTf)_2$ thus resulted in the regeneration of the original cage **Zn-1** or **Co-1**, as shown in Figures 3A and Figures S34 and S39.

The addition of fluoride to **2** produced similar results as for **1**, as shown in Figure 3B and Figures S36 and S40. Signals belonging to free 2-formyl-5-methoxypyridine were observed in the ^{1}H NMR spectrum after the addition of only 6 equiv of TBAF, *i.e.* 2 equiv TBAF per bis-pyridyl(imine) chelated vertex, confirming the disassembly of **2**. The release of encapsulated Tf_2N^- from cage **2** was also confirmed by ^{19}F NMR spectroscopy (Figures S38 and S41). No ^{19}F signals were observed between −160 and −170 ppm, indicating that no B←F^- adduct was present. Similarly to cage **1**, the addition of Ca^{2+} resulted in the reformation of cage **2** by precipitation of CaF_2, resulting in the re-encapsulation of Tf_2N^- within reformed **2**.

Chloride-induced cage disassembly

As reported in other contexts, the biologically relevant chloride anion (Cl^-) could be used to induce cage disassembly[56,57] and conformational changes.[58-60] We investigated the chloride-triggered disassembly of **1** and **2** by NMR (Figures S42-S47). As with fluoride addition, after the addition of tetrabutylammonium chloride (TBACl, 24 equiv) to **Zn-1** in CD_3CN, *i.e.* 2 equiv Cl^- per bis-pyridyl(imine) chelated vertex, the solution lightened in yellow colour and developed a precipitate. The ^{1}H NMR signals became broad, and signals corresponding to free 2-formyl-5-methoxy-pyridine were observed, suggesting cage disassembly. After the addition of TBACl (48 equiv) to **Co-1** in CD_3CN, *i.e.* 4 equiv TBACl per bis-pyridyl(imine) chelated vertex, the solution colour changed from yellow to light blue and developed a precipitate, consistent with the formation of $[CoCl_4]^{2-}$ and cage disassembly.

The addition of chloride to **2** produced similar results as for **1**. Signals belonging to free 2-formyl-5-methoxypyridine were observed in the ^{1}H NMR spectrum after the addition of only 6 equiv of TBACl, *i.e*. 2 equiv TBACl per bis-pyridyl(imine) chelated vertex, confirming the disassembly of **2**. The release of encapsulated Tf_2N^- from cage **2** was also confirmed by ^{19}F NMR spectroscopy (Figures S44 and S47).

Anion and metal ion induced structural transformations between cages

We hypothesised that **2** might transform into **1** following the addition of triflate or perchlorate and additional metal ions, through the displacement of Tf_2N^- from **2**. The addition of 3 equivalents of Zn^{II} and 20 equivalents of TfO^- thus effected the transformation of **Zn-2** into **Zn-1** (Figure 3C, Signal III). We infer that the Tf_2N^- templates within **Zn-2** were removed by excess TfO^- (Figure S32). Similarly, **Co-2** transformed into **Co-1** following the addition of 3 equivalents of Co^{II} and 20 equivalents of ClO_4^- (Figure S33).

Subcomponent exchange induced structural transformations

Subcomponent exchange has been shown[37] to effect transformations between cages. Compound 2-formyl-5-methoxypyridine was reported to form a Zn_6L_4 *pseudo*-octahedral cage **Zn-3** with subcomponent **A** (Figures S26-S31),[43] hence we investigated its effect on the cages considered in the present study with the addition of 2-formyl-1,10-phenanthroline (24 equiv) to **Zn-1** in CD_3CN (Signal IV in Figure 3C). After 24 h at 333 K, a set of peaks corresponding to *pseudo*-octahedral **Zn-3**[43] appeared (Figure S48). We infer that the formation of **Zn-3** is enthalpically favored due to the stronger coordination of its tridentate ligand arms to Zn^{II} in **Zn-3** compared with the bidentate ligand arms in **Zn-1**. **Co-1** likewise transformed into **Co-3** following 2-formyl-1,10-phenanthroline addition, as shown in Figure S51.

Zn-2 similarly transformed into **Zn-3** following the addition of 5-methoxypicolinaldehyde (24 equiv) and Zn^{II} (3 equiv) (Signal V in Figure 3C, Figure S49. The Tf_2N^- encapsulated in the cavity of **Zn-2** was released during the transformation from **Zn-2** to **Zn-3**, as evidenced by the disappearance of the ^{19}F signal at -78.5 ppm (Figure S50). **Co-2** likewise transformed into **Co-3** following a similar procedure as for **Zn-2**, (Figures S52 and S53).

Guest binding and regulation of paclitaxel uptake and release

Zn-1 and **Co-1** both bound a variety of guests, including neutral *C*-methylcalix[4]resorcinarene (**G1**) and anionic $B(C_6H_4F)_4^-$ (**G2**), in fast exchange on the NMR time scale (Figures S54-S61, S70 and S71). ESI-MS data (Figures S62-S65) suggested multiple binding of these guests to **Zn-1** and **Co-1**, as has been observed for other large cages;[61] their small NMR chemical shift displacements during binding (Figures S54 and S58) and uncertain binding stoichiometry precluded meaningful quantification of their binding constants. A possible binding mode where the guests protrude partially through the cage portals was suggested by MM3 modelling using the Scigress software package,[62] as depicted in Figure S76.

Co-1 was observed to bind the anti-cancer drug paclitaxel (**G3**). Host-guest binding was confirmed through progressive shifts in ^{1}H NMR peaks corresponding to both **Co-1** and **G3** (Figures S58 and S61). A 1:1 binding mode between **Co-1** and **G3** was supported by the ESI-MS spectrum (Figures S66 and S67). Isothermal Titration Calorimetry (ITC) was empolyed to measure the binding constant of **G3** and **Co-1**, yielding a value of $(4.6 \pm 0.2) \times 10^2$ M^{-1} (Figure S68). The diffusion coefficient for **G3** was found to be 1.02×10^{-5} cm^2 s^{-1}, and the diffusion coefficient for the bound guest **G3⊂Co-1** was 8.46×10^{-6} cm^2 s^{-1}, consistent with fast-exchange host-guest binding, as the value is smaller than that for free **G3** (Figure S69). An internal cavity volume of 1794 Å^3 for **Co-1** was calculated using MoloVol (Figure S75),[63] and is sufficient to accommodate the 768 Å^3 volume of **G3** with additional free volume that increases the binding entropy.[64] A possible configuration of **G3⊂Co-1** was visualised by MM3 modelling using the Scigress software package,[62] as depicted in Figure 4A.

The reversible fluoride-triggered disassembly of cage **1** drove paclitaxel release and uptake within host **Co-1**. As shown in Figure 4B and Figures S72 and S73, upon the addition of fluoride (24 equiv) to **G3⊂Co-1** in CD_3CN, the colour of the solution changed from light to dark orange.

Fluoride addition was observed to induce the release of **G3**, as confirmed by ^{1}H NMR spectroscopy. Subsequent addition of Ca^{2+} (48 equiv) to fluoride-disassembled **G3** stimulated the reformation of the host-guest complex **G3⊂Co-1** (Figures S72 and S73). Cage **1** also disassembled when treated with chloride, leading to the release of paclitaxel within host **Co-1**, was also investigated, as shown in Figure S74. The use of chloride, which is more biocompatible than fluoride, may have more relevance for drug delivery. These results highlight potential applications for these cages in natural product separations and drug delivery.

CONCLUSIONS

Pseudo-cuboctahedral **1** and *pseudo*-Johnson-type (J_{51}) **2** form parts of a network of coordination cages that interconvert in response to chemical stimuli, including fluoride, weakly coordinating anions, and aldehyde subcomponents. These interconversions regulate the binding of guests, including paclitaxel, suggesting potential applications in natural product separation and drug delivery. The incorporation of bis-pyridyl(imine) chelated octahedral metal vertices into coordination cages, using principles developed in this work, may also pave the way to the design and construction of new lower-symmetry coordination cages. The reversible opening of these coordination cages in response to fluoride, in contrast to cages containing tris-pyridyl(imine) metal vertices, might be useful in the context of systems of cages that respond in complex ways to different signals.

EXPERIMENTAL PROCEDURES

Resource availability

Lead contact

Further information and requests for resources and reagents should be directed to the lead contact, Jonathan R. Nitschke (jrn34@cam.ac.uk).

Materials availability

This study did not generate new unique reagents.

Data and code availability

The accession numbers for the crystallographic data reported in this paper are CCDC: 2301542 (**Zn-1**). Copies of these data can be obtained free of charge from the Cambridge Crystallographic Data Centre via www.ccdc.cam.ac.uk/data_request/cif. Correspondence and requests for materials should be addressed to J.R.N.. The OPTIM and GMIN programs are available for download from www-wales.ch.cam.ac.uk under the Gnu General Public License.

Full experimental procedures are provided in the supplemental information.

SUPPLEMENTAL INFORMATION

Supplemental information can be found online at https://doi.org/10.1016/j.chempr.xxxxx.

ACKNOWLEDGMENTS

This study was supported by the European Research Council (695009) and the UK Engineering and Physical Sciences Research Council (EPSRC, EP/T031603/1, EP/P027067/1, and EP/S024220/1). J.Z. acknowledges the Cambridge Trust and Newnham College for PhD funding. We thank the Department of Chemistry NMR facility, University of Cambridge, for performing some NMR experiments, and Diamond Light Source (UK) for synchrotron beamtime on I19 (CY29890). We also thank Natasha Speakman for useful discussions and Philipp Pracht for advice with the calculations.

AUTHOR CONTRIBUTIONS

J.R.N. and Y.Y. conceived the project and designed the experiments. Y.Y. and Y.D. performed the experiments and analyzed the data. P.C.P.T. and D.J.W. performed the GFN2-xTB calculations. J.Z. collected the X-ray data and T.K.R. refined the crystal structure. Y.Y. and P.C.P.T. drafted and edited the manuscript. J.R.N. is the principal investigator. All authors discussed the results and commented on the manuscript.

DECLARATION OF INTERESTS

The authors declare no competing interests.

REFERENCES

1. Chakrabarty, R., Mukherjee, P.S., and Stang, P.J. (2011). Supramolecular coordination: Self-assembly of finite two- and three-dimensional ensembles. Chem. Rev., 111, 6810–6918. 10.1021/cr200077m.
2. Smulders, M.M.J., Riddell, I.A., Browne, C., and Nitschke, J.R. (2013). Building on architectural principles for three-dimensional metallosupramolecular construction. Chem. Soc. Rev., 42, 1728–1754. 10.1039/c2cs35254k.
3. Zhang, G., and Mastalerz, M. (2014). Organic cage compounds – from shape-persistency to function. Chem. Soc. Rev., 43, 1934–1947. 10.1039/C3CS60358J.
4. Fujita, D., Ueda, Y., Sato, S., Yokoyama, H., Mizuno, N., Kumasaka, T., and Fujita, M. (2016). Self-Assembly of $M_{30}L_{60}$ Icosidodecahedron. Chem, 1, 91–101. 10.1016/j.chempr.2016.06.007.
5. Koo, J., Kim, I., Kim, Y., Cho, D., Hwang, I.C., Mukhopadhyay, R.D., Song, H., Ko, Y.H., Dhamija, A., Lee, H., et al. (2020). Gigantic porphyrinic cages. Chem, 6, 3374–3384. 10.1016/j.chempr.2020.10.002.
6. Liu, Y., Hu, C., Comotti, A., and Ward, M.D. (2011). Supramolecular archimedean cages assembled with 72 hydrogen bonds. Science, 333, 436–440. 10.1126/science.1204369.
7. Pasquale, S., Sattin, S., Escudero-Adán, E.C., Martínez-Belmonte, M., and De Mendoza, J. (2012). Giant regular polyhedra from calixarene carboxylates and uranyl. Nat. Commun., 3, 785. 10.1038/ncomms1793.
8. Wang, H., Wang, K., Xu, Y., Wang, W., Chen, S., Hart, M., Wojtas, L., Zhou, L.-P., Gan, L., Yan, X., et al. (2021). Hierarchical self-assembly of nanowires on the surface by metallo-supramolecular truncated cuboctahedra. J. Am. Chem. Soc., 143, 5826–5835. 10.1021/jacs.1c00625.
9. Chen, Y.S., Solel, E., Huang, Y.F., Wang, C.L., Tu, T.H., Keinan, E., and Chan, Y.T. (2019). Chemical mimicry of viral capsid self-assembly via corannulene-based pentatopic tectons. Nat. Commun., 10, 3443. 10.1038/s41467-019-11457-6.
10. Wu, K., Ronson, T.K., Su, P., Chen, Z., Goh, L., Heard, A.W., Li, X., Klautzsch, F., Schalley, C.A., Vinković, M., et al. (2023). Systematic construction of progressively larger capsules from a fivefold linking pyrrole-based subcomponent. Nat. Synth., 2, 789–797. 10.1038/s44160-023-00276-9.
11. Luo, D., Wang, X.Z., Yang, C., Zhou, X.P., and Li, D. (2018). Self-assembly of chiral metal-organic tetartoid. J. Am. Chem. Soc., 140, 118–121. 10.1021/jacs.7b11285.
12. Fu, Q., Li, W.-X., Yao, Y., Liu, H., Su, H.-Y., Ding, M., Gu, X.-K., Chen, L., Wang, Z., Zhang, H., et al. (2010). Interface-confined ferrous centers for catalytic oxidation. Science, 328, 1141–1144. 10.1126/science.1188267.
13. Olenyuk, B., Levin, M.D., Whiteford, J.A., Shield, J.E., and Stang, P.J. (1999). Self-assembly of nanoscopic dodecahedra from 50 predesigned components. J. Am. Chem. Soc., 121, 10434–10435. 10.1021/ja9931933.
14. Rizzuto, F.J., Carpenter, J.P., and Nitschke, J.R. (2019). Multisite binding of drugs and natural products in an entropically favorable, heteroleptic receptor. J. Am. Chem. Soc., 141, 9087–9095. 10.1021/jacs.9b03776.
15. Li, B., Zhang, W., Lu, S., Zheng, B., Zhang, D., Li, A., Li, X., Yang, X.-J., and Wu, B. (2020). Multiple transformations among anion-based $A_{2n}L_{3n}$ assemblies: Bicapped trigonal antiprism A_8L_{12}, tetrahedron A_4L_6, and triple helicate A_2L_3 (A = anion). J. Am. Chem. Soc., 142, 21160–21168. 10.1021/jacs.0c10346.
16. Grimes, J.M., Burroughs, J.N., Gouet, P., Diprose, J.M., Malby, R., Ziéntara, S., Mertens, P.P.C., and Stuart, D.I. (1998). The atomic structure of the bluetongue virus core. Nature, 395, 470–478. 10.1038/26694.
17. Johnson, N.W. (1966). Convex polyhedra with regular faces. Can. J. Math., 18, 169–200. 10.4153/cjm-1966-021-8.
18. Cromwell, P.R. (2017). Polyhedra: One of the most charming chapters of geometry. Cambridge University Press.
19. Mal, P., Breiner, B., Rissanen, K., and Nitschke, J.R. (2009). White phosphorus is air-stable within a self-assembled tetrahedral capsule. Science, 324, 1697–1699. 10.1126/science.1175313.
20. Huang, B., Mao, L., Shi, X., and Yang, H.-B. (2021). Recent advances and perspectives on supramolecular radical cages. Chem. Sci., 12, 13648–13663. 10.1039/d1sc01618k.
21. García-Simón, C., Garcia-Borràs, M., Gómez, L., Parella, T., Osuna, S., Juanhuix, J., Imaz, I., Maspoch, D., Costas, M., and Ribas, X. (2014). Sponge-like molecular cage for purification of fullerenes. Nat. Commun. 5, 5557. 10.1038/ncomms6557.
22. Zhang, D., Ronson, T.K., Zou, Y.Q., and Nitschke, J.R. (2021). Metal–organic cages for molecular separations. Nat. Rev. Chem., 5, 168–182. 10.1038/s41570-020-00246-1.
23. Fuertes-Espinosa, C., Pujals, M., and Ribas, X. (2020). Supramolecular purification and regioselective functionalization of fullerenes and endohedral metallofullerenes. Chem, 6, 3219–3262. 10.1016/j.chempr.2020.11.003

24. Chen, L.-J., Yang, H.-B., and Shionoya, M. (2017). Chiral metallosupramolecular architectures. Chem. Soc. Rev., 46, 2555–2576. 10.1039/c7cs00173h.

25. Dong, J., Liu, Y., and Cui, Y. (2021). Supramolecular chirality in metal-organic complexes. Acc. Chem. Res., 54, 194–206. 10.1021/acs.accounts.0c00604.

26. Takezawa, H., Shitozawa, K., and Fujita, M. (2020). Enhanced reactivity of twisted amides inside a molecular cage. Nat. Chem., 12, 574–578. 10.1038/s41557-020-0455-y.

27. Ward, M.D., Hunter, C.A., and Williams, N.H. (2018). Coordination cages based on bis(pyrazolylpyridine) ligands: structures, dynamic behavior, guest binding, and catalysis. Acc. Chem. Res., 51, 2073–2082. 10.1021/acs.accounts.8b00261.

28. Nakabayashi, K., Kawano, M., and Fujita, M. (2005). pH-Switchable through-space interaction of organic radicals within a selfassembled coordination cage. Angew. Chem. Int. Ed., 44, 5322–5325. 10. 1002/anie.200501568.

29. Sivalingam, V., Parbin, M., Krishnaswamy, S. and Chand, D.K. (2024). Cage-to-cage transformations in self-assembled coordination cages using “acid/base” or “guest binding-induced strain” as stimuli. Angew. Chem. Int. Ed., 63, e202403711. 10.1002/anie.202403711.

30. Lee, H., Tessarolo, J., Langbehn, D., Baksi, A., Herges, R., and Clever, G.H. (2022). Light powered dissipative assembly of diazocine coordination cages. J. Am. Chem. Soc., 144, 3099–3105. 10.1021/jacs. 1c12011.

31. DiNardi, R. G., Douglas, A. O., Tian, R., Price, J. R., Tajik, M., Donald, W. A. and Beves, J. E. (2022). Visible-light-responsive self-assembled complexes: improved photoswitching properties by metal ion coordination. Angew. Chem. Int. Ed., 61, e202205701. 10.1002/anie.202205701.

32. Kennedy, A. D. W., DiNardi, R. G., Fillbrook, L. L., Donald, W. A. and Beves, J. E. (2022). Visible-light switching of metallosupramolecular assemblies. Chem. Eur. J., 28, e202104461. 10.1002/chem.202104461.

33. Samanta, D., Galaktionova, D., Gemen, J., Shimon, L.J.W., Diskin-Posner, Y., Avram, L., Král, P., and Klajn, R. (2018). Reversible chromism of spiropyran in the cavity of a flexible coordination cage. Nat. Commun., 9, 641. 10.1038/s41467-017-02715-6.

34. Ronson, T.K., Carpenter, J.P., and Nitschke, J.R. (2022). Dynamic optimization of guest binding in a library of diastereomeric heteroleptic coordination cages. Chem, 8, 557–568. 10.1016/j.chempr.2021.12.017.

35. Hema, K., Grommet, A.B., Białek, M.J., Wang, J., Schneider, L., Drechsler, C., Yanshyna, O., Diskin-Posner, Y., Clever, G.H., and Klajn, R. (2023). Guest encapsulation alters the thermodynamic landscape of a coordination host. J. Am. Chem. Soc., 145, 24755–24764. 10.1021/jacs.3c08666.

36. Walther, A., Regeni, I., Holstein, J. J., and Clever, G. H. (2023). Guest-induced reversible transformation between an azulene-based Pd_2L_4 lantern-shaped cage and a Pd_4L_8 tetrahedron. J. Am. Chem. Soc., 145, 25365–25371. 10.1021/jacs.3c09295

37. Zhang, D., Ronson, T.K., and Nitschke, J.R. (2018). Functional capsules via subcomponent self-assembly. Acc. Chem. Res., 51, 2423–2436. 10.1021/acs.accounts.8b00303.

38. Lisboa, L. S., Findlay, J. A., Wright, L. J., Hartinger, C. G., and Crowley, J. D. (2020). A reduced-symmetry heterobimetallic $[PdPtL_4]^{4+}$ cage: Assembly, guest binding, and stimulus-induced switching. Angew. Chem. Int. Ed., 59, 11101–11107. 10.1002/anie.202003220.

39. Bandi, S. and Chand, D. K. (2016). Cage-to-cage cascade transformations. Chem. Eur. J., 22, 10330–10335. 10.1002/chem.201602039.

40. Vasdev, R. A. S., Findlay, J. A., Garden, A. L., and Crowley, J. D. (2019). Redox active $[Pd_2L_4]^{4+}$ cages constructed from rotationally flexible 1,1'-disubstituted ferrocene ligands. Chem. Commun., 55, 7506–7509. 10.1039/c9cc03321a.

41. Yang, Y., Du, Y., Ronson, T. K., and Nitschke, J. R. (2024). Steric control over interligand dihedrals and splay leads to the formation of $Fe^{II}_6L_6$ and $Fe^{II}_8L_8$ antiprisms. CCS Chem. 10.31635/ccschem.024.202404281

42. Liu, J., Wang, Z., Cheng, P., Zaworotko, M.J., Chen, Y., and Zhang, Z. (2022). Post-synthetic modifications of metal–organic cages. Nat. Rev. Chem., 6, 339–356. 10.1038/s41570-022-00380-y.

43. Yang, Y., Ronson, T.K., Zheng, J., Mihara, N., and Nitschke, J.R. (2023). Fluoride up- and down-regulates guest encapsulation for $Zn^{II}_6L_4$ and $Zn^{II}_4L_4$ cages. Chem, 9, 1972–1982. 10.1016/j.chempr.2023.03.027.

44. Yang, Y., Ronson, T.K., Hou, D., Zheng, J., Jahović, I., Luo, K.H., and Nitschke, J.R. (2023). Hetero-diels–alder reaction between singlet oxygen and anthracene drives integrative cage self-sorting. J. Am. Chem. Soc., 145, 19164–19170. 10.1021/jacs.3c04228.

45. Luo, D., Yuan, Z.-J., Ping, L.-J., Zhu, X.-W., Zheng, J., Zhou, C.-W., Zhou, X.-C., Zhou, X.-P. and Li, D. (2023) Tailor-made Pd_nL_{2n} metal-organic cages through covalent post-synthetic modification. Angew. Chem. Int. Ed., 62, e2022169. 10.1002/anie.202216977.

46. Jiang, W.-L., Huang, B., Zhao, X.-L., Shi, X., and Yang, H.-B. (2023). Strong halide anion binding within the cavity of a conformation-adaptive phenazine-based Pd_2L_4 cage. Chem., 9, 2655–2668. 10.1016/j.chempr.2023.06.020.

47. Freye, S., Michel, R., Stalke, D., Pawliczek, M., Frauendorf, H., and Clever, G. H. (2013). Template control over dimerization and guest selectivity of interpenetrated

coordination cages. J. Am. Chem. Soc., 135, 8476–8479. 10.1021/ja403184a.

48. Hang, X., Liu, B., Zhu, X., Wang, S., Han, H., Liao, W., Liu, Y., and Hu, C. (2016). Discrete {Ni40} coordination cage: A calixarene-based Johnson-Type (J_{17}) hexadecahedron. J. Am. Chem. Soc., 138, 2969–2972. 10.1021/jacs.6B00695.
49. Wu, T., Jiang, Z., Bai, Q., Li, Y., Mao, S., Yu, H., Wojtas, L., Tang, Z., Chen, M., Zhang, Z., et al. (2021). Supramolecular triangular orthobicupola: Self-assembly of a giant Johnson solid J_{27}. Chem, 7, 2429–2441. 10.1016/j.chempr.2021.06.003.
50. Allan, D.R., Nowell, H., Barnett, S.A., Warren, M.R., Wilcox, A., Christensen, J., Saunders, L.K., Peach, A., Hooper, M.T., Zaja, L., et al. (2017). A novel dual air-bearing fixed-χ diffractometer for small-molecule single-crystal X-ray diffraction on beamline I_{19} at diamond light source. Crystals (Basel) 7, 336. 10.3390/cryst7110336.
51. Rizzuto, F.J. and Nitschke, J.R. (2017). Stereochemical plasticity modulates cooperative binding in a $Co^{II}_{12}L_6$ cuboctahedron. Nat. Chem., 9, 903-908. 10.1038/nchem.2758.
52. Nakamura, T., Ube, H., Miyake, R., and Shionoya, M. (2013). A C_{60} -templated tetrameric porphyrin barrel complex via zinc-mediated self-assembly utilizing labile capping ligands. J. Am. Chem. Soc., 135, 18790–18793. 10.1021/ja4110446.
53. Nakamura, T., Ube, H., Shiro, M., and Shionoya, M. (2013). A self‐assembled multiporphyrin cage complex through three different Zinc(II) center formation under well-balanced aqueous conditions. Angew. Chem. Int. Ed., 52, 720–723 10.1002/anie.201208040.
54. Lehr, M., Paschelke, T., Trumpf, E., Vogt, A., Näther, C., Sönnichsen, F.D., and McConnell, A.J. (2020). A paramagnetic NMR spectroscopy toolbox for the characterisation of paramagnetic/spin‐crossover coordination complexes and metal‐organic cages. Angew. Chem. Int. Ed., 59, 19344–19351. 10.1002/anie.202008439.
55. Wesołowski P.A., Wales D.J. and Pracht P. A (2024). Multilevel Framework for Analysis of Protein Folding Involving Disulphide Bond Formation. J. Phys. Chem. B, 128, 3145−3156. 10.1021/acs.jpcb.4c00104.
56. Lewis, J. E. M., Gavey, E. L., Camerona, S. A., and Crowley, J. D. (2012). Stimuli-responsive Pd_2L_4 metallosupramolecular cages: towards targeted cisplatin drug delivery. Chem. Sci., 3, 778-784. 10.1039/C2SC00899H.
57. Preston, D., Fox-Charles, A., Lo, W. K. C., and Crowley, J. D. (2015). Chloride triggered reversible switching from a metallosupramolecular $[Pd_2L_4]^{4+}$ cage to a $[Pd_2L_2Cl_4]$ metallo-macrocycle with release of *endo*- and *exo*-hedrally bound guests. Chem. Commun., 51, 9042-9045. 10.1039/C5CC02226F.
58. Zhu, R., Lübben, J., Dittrich, B., and Clever, G. H. (2015). Stepwise halide-triggered double and triple catenation of self-assembled coordination cages. Angew. Chem. Int. Ed., 54, 2796 –2800. 10.1002/anie.201408068.
59. Jurček, O., Bonakdarzadeh, P., Kalenius, E., Linnanto, J. M., Groessl, M., Knochenmuss, R., Ihalainen, J. A., and Rissanen, K. (2015). Superchiral Pd_3L_6 coordination complex and its reversible structural conversion into $Pd_3L_3Cl_6$ metallocycles. Angew. Chem. Int. Ed., 54, 15462 –15467. 10.1002/anie.201506539.
60. Endo, K., Ube, H., and Shionoya, M. (2020). Multi-stimuli-responsive interconversion between bowl- and capsule-shaped self-assembled Zinc(II) complexes. J. Am. Chem. Soc., 142, 407–416. 10.1021/jacs.9b11099.
61. Wu, K., Ronson, T.K., Goh, L., Xue, W., Heard, A.W., Su, P., Li, X., Vinković, M., and Nitschke, J.R. (2023). A diverse array of large capsules transform in response to stimuli. J. Am. Chem. Soc., 145, 11356–11363. 10.1021/jacs.3c02491.
62. Geometry optimised structures were modelled using the MM3 force field on SCIGRESS software (Fujitsu Limited, Tokyo, Japan, 2013) version FJ 2.6 (EU 3.1.9) Build 5996.8255.20141202.
63. Maglic, J.B., and Lavendomme, R. (2022). MoloVol: An easy-to-use program for analyzing cavities, volumes and surface areas of chemical structures. J. Appl. Crystallogr., 55, 1033–1044. 10.1107/S1600576722004988.
64. Mecozzi, S., and Rebek, Jr., J. (1998). The 55 % solution: A formula for molecular recognition in the liquid state. Chem. Eur. J., 4, 1016–1022. 10.1002/(SICI)1521-3765(19980615)4:6<1016::AID-CHEM1016>3.0.CO;2-B.

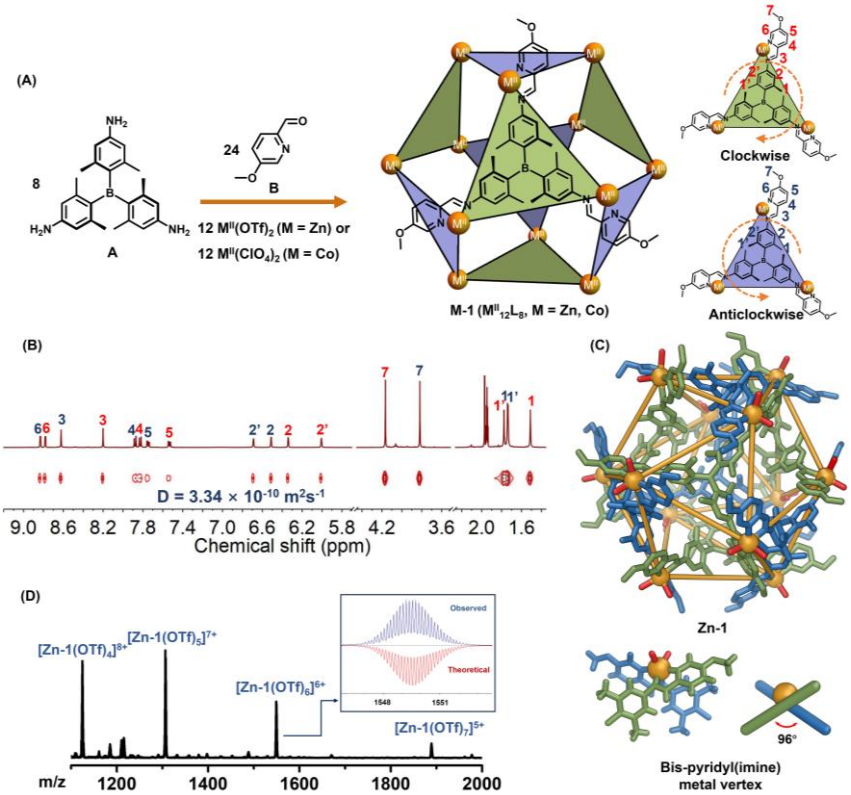

Figure 1. Self-assembly of 1.

(A) Self-assembly of **Zn-1** and **Co-1**, showing the clockwise and anticlockwise orientations observed in the crystal of the outward-facing ligand methyl groups in both types of cage faces.
(B) ^{1}H NMR spectrum (400 MHz, CD_3CN, 298 K) and DOSY spectrum of **Zn-1**.

(C) Crystal structure of **Zn-1** (acetonitrile and counterions coordinated to the metal vertices are shown as red sticks).

(D) ESI-MS of **Zn-1**.

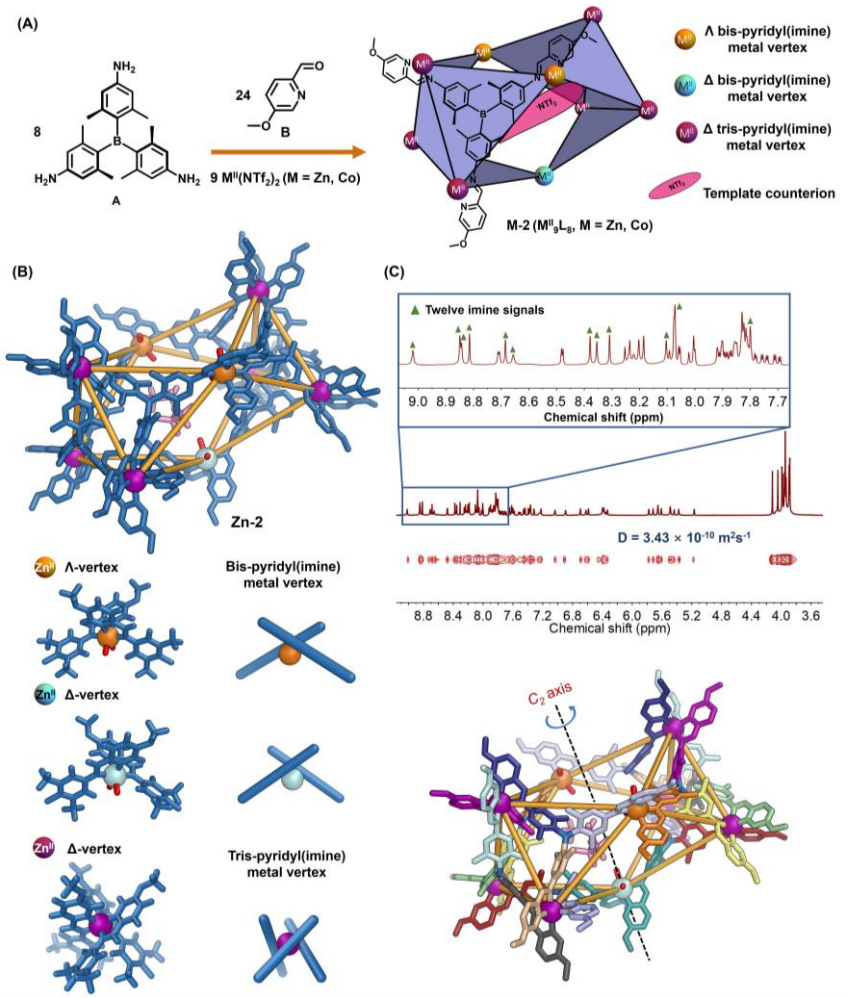

Figure 2. Self-assembly and characterization of 2.

(A) Subcomponent self-assembly of **Zn-2** and **Co-2. Zn-2** and **Co-2** formed only in the presence of Tf_2N^-, indicating that Tf_2N^- may serve the role of a template during formation of the framework of **2**.

(B) GFN2-xTB -optimized[51] structure of **Zn-2**, with putative monodentate ligands coordinated to metal vertices shown as red sticks.

(C) ^{1}H NMR, DOSY spectra of **Zn-2**, and chematic illustration of **Zn-2** showing the C_2 axis, with chemically distinct ligand arm environments colored differently.

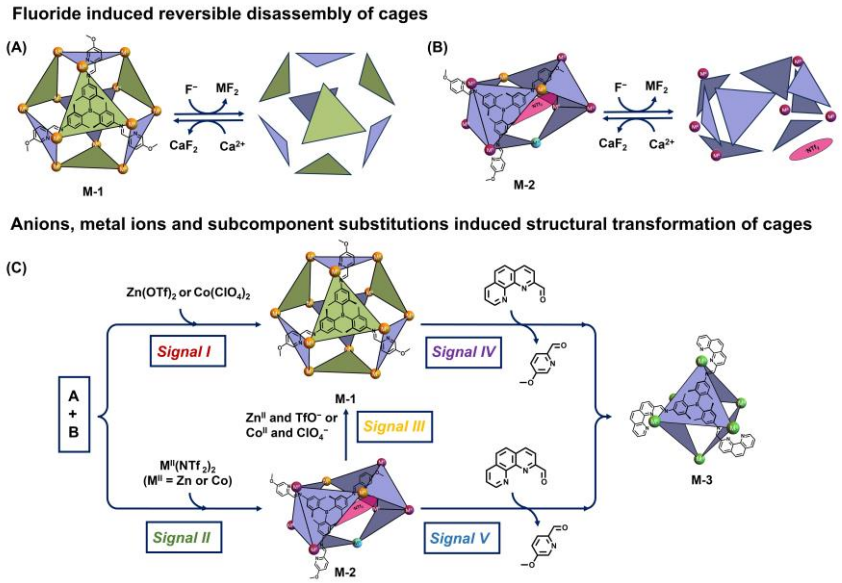

Figure 3. Structural transformations of cages.

(A) Fluoride-induced reversible disassembly of **M-1**.

(B) Fluoride-induced reversible disassembly of **M-2**.

(C) Added anions, metal ions, and aldehyde subcomponents induce structural transformations between **M-1**, **M-2**, and **M-3**.[43] The signals are I, $Zn^{II}(OTf)_2$ or $Co^{II}(ClO_4)_2$ at 65 °C for 12 h; II, $Zn(NTf_2)_2$ or $Co(NTf_2)_2$ at 65 °C for 12 h; III, Zn^{II} and excess TfO^-, or Co^{II} and excess ClO_4^- heating at 50 °C for 3 h; IV, 2-formyl-1,10-phenanthroline, heating at 65 °C for 12 h; V, 2-formyl-1,10-phenanthroline and Zn^{II} or Co^{II}, heating at 65 °C for 12 h.

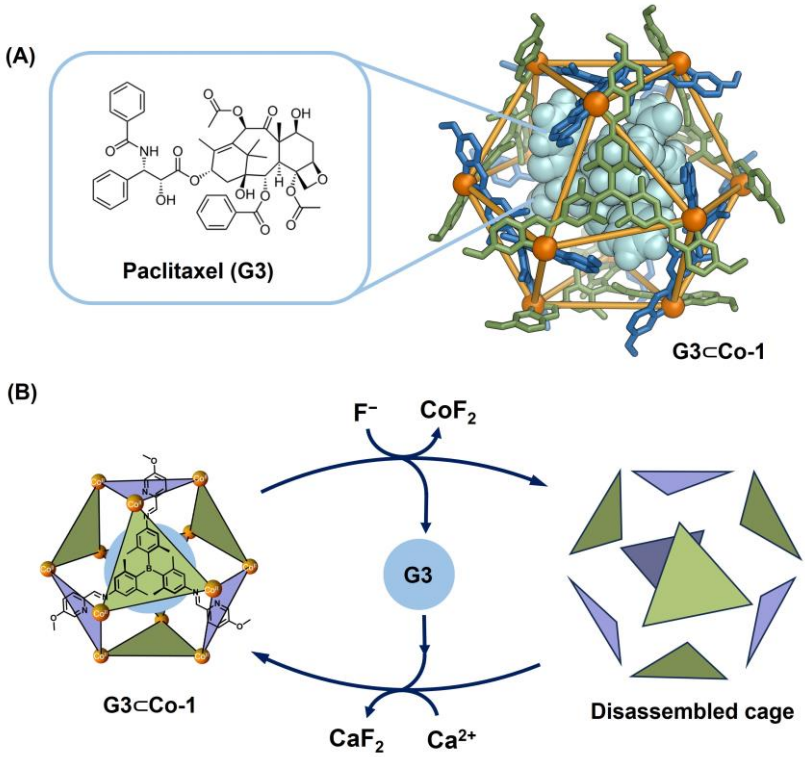

Figure 4. Regulation of paclitaxel uptake and release

(A) Modelled structure for host-guest complex **G3⊂Co-1** based upon the crystal structure of **Zn-1.**
(B) **G3** was released from **G3⊂Co-1** upon fluoride-stimulated cage opening and taken up again upon Ca^{2+}-stimulated cage reformation.

TOC